



Water on Hot Rocky Exoplanets

Edwin S. Kite¹ and Laura Schaefer²

¹ Department of the Geophysical Sciences, University of Chicago, Chicago, IL, USA; kite@uchicago.edu

² School of Earth Sciences, Stanford University, Palo Alto, CA, USA

Received 2020 December 22; revised 2021 February 8; accepted 2021 February 18; published 2021 March 15

Abstract

Data suggest that most rocky exoplanets with orbital period $p < 100$ days (“hot” rocky exoplanets) formed as gas-rich sub-Neptunes that subsequently lost most of their envelopes, but whether these rocky exoplanets still have atmospheres is unknown. We identify a pathway by which $1\text{--}1.7 R_{\oplus}$ ($1\text{--}10 M_{\oplus}$) rocky exoplanets with orbital periods of 10–100 days can acquire long-lived 10–2000 bar atmospheres that are H_2O -dominated, with mean molecular weight >10 . These atmospheres form during the planets’ evolution from sub-Neptunes into rocky exoplanets. H_2O that is made by reduction of iron oxides in the silicate magma is highly soluble in the magma, forming a dissolved reservoir that is protected from loss so long as the H_2 -dominated atmosphere persists. The large size of the dissolved reservoir buffers the H_2O atmosphere against loss after the H_2 has dispersed. Within our model, a long-lived, water-dominated atmosphere is a common outcome for efficient interaction between a nebula-derived atmosphere (peak atmosphere mass fraction 0.1–0.6 wt%) and oxidized magma (>5 wt% FeO), followed by atmospheric loss. This idea predicts that most rocky planets that have orbital periods of 10–100 days and that have radii within $0.1\text{--}0.2 R_{\oplus}$ of the lower edge of the radius valley still retain H_2O atmospheres. This prediction is imminently testable with James Webb Space Telescope and has implications for the interpretation of data for transiting super-Earths.

Unified Astronomy Thesaurus concepts: [Extrasolar rocky planets \(511\)](#); [Exoplanet atmospheres \(487\)](#); [Exoplanet evolution \(491\)](#)

1. Introduction

Most Sun-like stars are orbited by a hot rocky exoplanet—a world with orbital period $p < 100$ days, radius $R < 1.7 R_{\oplus}$, and a density indicating that it is mostly composed of Fe-metal and silicates (Dai et al. 2019; Hsu et al. 2019; Otegi et al. 2020). The question “do these worlds have atmospheres?” defines the observational frontier for rocky-exoplanet research (e.g., Koll et al. 2019; Kreidberg et al. 2019). For example, searches for high-molecular-weight atmospheres on hot rocky exoplanets will be possible using the James Webb Space Telescope. Data suggest that $\sim 80\%$ of hot super-Earths formed as sub-Neptunes, with thick nebula-derived atmospheres of H_2 overlying silicate magma, and that the H_2 envelope (atmosphere mass fraction f_{atm} up to 1 wt% of planet mass) was removed by atmosphere loss to space (e.g., Rogers & Owen 2020). Here we define a “super-Earth” as a world with $1 R_{\oplus} < R < 1.7 R_{\oplus}$, and a “sub-Neptune” as a world with $1.8 R_{\oplus} < R < 4 R_{\oplus}$. The apparent near-ubiquity of an atmospheric loss process powerful enough to halve planet volume suggests that super-Earths that formed as sub-Neptunes would not have a nebula-derived atmosphere today. In other words, the prevailing view is that observing a rocky super-Earth with a thin (<500 km thick) nebula-derived atmosphere would require fine-tuning, either of the time of cessation of the atmosphere loss process, or of the time of observation relative to the planet’s evolution.

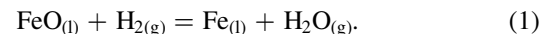
Thus, previously proposed routes by which a hot rocky super-Earth might acquire an atmosphere have focused on solid-derived volatiles (involving volatile-rich bolides, e.g., Bitsch et al. 2019, or volcanism from a volatile-bearing interior, e.g., Kite & Barnett 2020). Whether or not these mechanisms robustly lead to atmospheres on hot rocky exoplanets depends on the details of volatile transport from colder regions of the exoplanetary system. These mechanisms do not require an initial

atmosphere of nebula-derived H_2 . These mechanisms would work as well or better for planets that formed without such an atmosphere (“intrinsically rocky” worlds).

By contrast, in this study we explore a pathway that only endows rocky planets with atmospheres if those planets are born with thick H_2 envelopes.³ Specifically, we investigate a pathway by which atmospheric escape distills the products of chemical reactions between silicate magma and nebula-derived H_2 to yield hot rocky exoplanets with 10–2000 bar, long-lived H_2O atmospheres. Surprisingly, as we will show, this distillation happens even when the atmospheric escape is itself unfractionating.

2. Method

Our method shares the assumptions of Kite et al. (2020), with the major change being the incorporation of atmospheric escape in the present study. Kite et al. (2020) calculate magma–atmosphere equilibration in the Fe–Mg–Si–O–H system, neglecting Fe^{3+} and He, and assuming that volatiles equilibrate with magma at $T \sim 2500$ K. H_2 from the nebula is oxidized by magmatic Fe^{2+}O to form H_2O (this has previously been proposed as a way to form oceans on habitable-zone planets; e.g., Sasaki 1990; Ikoma & Genda 2006). The key reaction is



Following Kite et al. (2020), we assume here that the initial nebula-derived atmosphere chemically equilibrates with a well-stirred magma ocean at the pressure and temperature of the magma–atmosphere interface. Using the wide range of pre-volatile-equilibration magma FeO weight fractions that is plausible for exoplanets (Elkins-Tanton & Seager 2008b;

³ In this study, we use the terms “atmosphere” and “envelope” as synonyms.

Doyle et al. 2020), the resulting $\text{H}_2/\text{H}_2\text{O}$ atmosphere has a mean molecular weight (μ_{atm}) of 2–7 Da (Kite et al. 2020). Fe^{2+} reduction yields liquid metal (Fe^0), which is insoluble in magma, and sinks to the planet’s center where (we assume) it is chemically isolated. Both H_2O and H_2 are soluble in magma, but there is a big contrast in the solubilities. Taking basaltic magma at 1 GPa as an example, in the presence of pure H_2O , H_2O solubility is 16 wt% (extrapolating Papale 1997), but in the presence of pure H_2 , H_2 solubility is only 0.57 wt% (Hirschmann et al. 2012).

A large fraction of the planet’s total H_2 is stored in the atmosphere, but almost all of the H_2O (10^{23} – 10^{24} kg, equivalent to 10^2 – 10^3 Earth oceans) is stored in the magma. This is much larger than the mass of other volatile species, such as C, which we neglect.

In this study we ask: *Under atmospheric loss, does the H_2O escape to space, reoxidize the magma, or stay as a H_2O envelope?* To answer this question, we first model atmospheric loss from the model planets calculated by Kite et al. (2020). (Loss could be via hydrodynamic escape, itself powered either by X-ray and extreme ultraviolet radiation from the star or by the luminosity of the silicate core, or via impact erosion; Bean et al. 2020.) We model bulk (nonfractionating) loss, as the atmosphere is too hot for water to condense or to unmix from H_2 , and the loss rate is thought to be too fast for diffusive separation of H_2 from H_2O to be important (e.g., Hu et al. 2015; Kite & Barnett 2020). (We return to the role of selective escape in Section 4.)

We carry out bulk removal of atmosphere from the planet via many small steps. After each small step of gas removal, we resolve for atmosphere–magma equilibrium partitioning of each of the two volatiles (H_2 and H_2O):

$$\begin{aligned} c_i &= e_i + p_i s_i m_{\text{magma}} \\ &= e_i + [(e_i/A_{\text{mai}})g(\mu_{\text{atm}}/\mu_i)]s_i m_{\text{magma}}. \end{aligned} \quad (2)$$

Here, c_i is the total inventory of the volatile i (decreasing at each step due to removal to space), e_i is the mass in the atmosphere, p_i is the partial pressure at the magma–atmosphere interface, and A_{mai} (and g) are the area of (and gravitational acceleration at) the magma–atmosphere interface. μ_{atm} is the mean molecular weight of the atmosphere, μ_i is the molecular weight of the volatile i , s_i is the solubility coefficient (mass fraction Pa^{-1}) of the volatile, and m_{magma} is the magma–ocean mass. Each step depressurizes the top of the magma ocean. Therefore, at each step some gas in the ocean is exsolved. Exsolution is a brake on thinning of the atmosphere ($\partial e_i/\partial c_i < 1$). This “brake” is more effective for H_2O than for H_2 because of the large mass of the dissolved-in-magma H_2O reservoir.

In general s_i varies with p_i and total pressure. For this study, we follow Schaefer et al. (2016) and set $s_{\text{H}_2\text{O}} = 3.44 \times 10^{-8} p_{\text{H}_2\text{O}}^{-0.26}$. We assume that s_{H_2} is equal throughout each simulation to its value at the maximum atmospheric pressure for each simulation. This overstates the shielding of H_2 within the magma. This is conservative relative to our conclusion that H_2O -dominated atmospheres emerge relatively early.

3. Results

Figure 1 shows results for a world with mass $M = 5 M_{\oplus}$ that initially has magma $X_{\text{FeO}} = 11$ wt%, similar to the FeO content of Earth’s mantle. In order to generate the initial condition (left

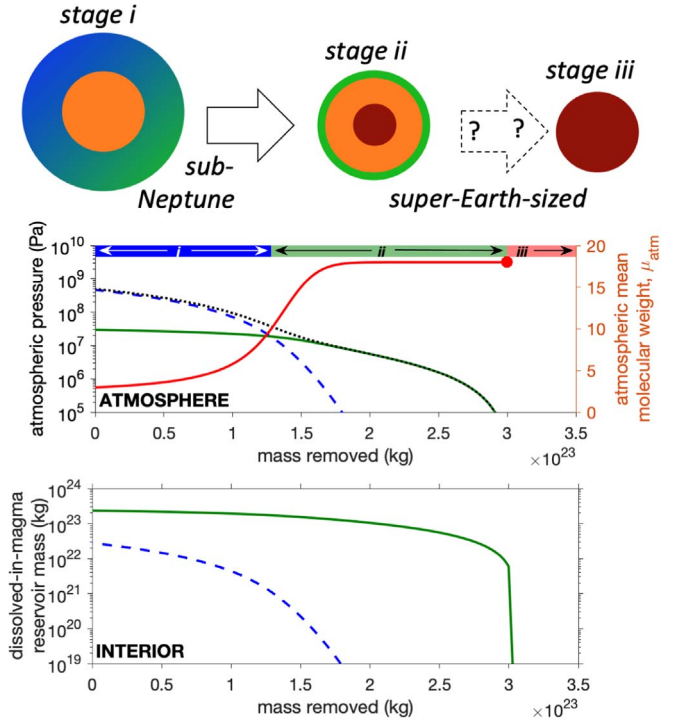


Figure 1. Example model output. Top row: overview of the modeled scenario: a sub-Neptune with a core of mass $5 M_{\oplus}$ that initially has FeO content similar to that of Earth’s mantle, then has H_2 added until the base of atmosphere pressure is 5 kbar (with magma–atmosphere equilibration) (stage i). Blue and green shading corresponds to atmospheric H_2 and atmospheric H_2O , respectively. Orange shading corresponds to liquid magma, and red shading corresponds to solid rock. The planet then undergoes nonfractionating (bulk) atmospheric loss and the atmosphere evolves into a H_2O atmosphere (stage ii). The Fe-metal core is not shown. Lower panels: the corresponding H_2 reservoirs (dashed blue lines), H_2O reservoirs (green lines), total atmospheric pressure (dotted line), and atmospheric mean molecular weight (red line) for this scenario. The blue bar (“i”) corresponds to the H_2 -dominated regime, the green bar (“ii”) corresponds to the H_2O -dominated regime, and the red bar (“iii”) corresponds to the bare-rock stage after all atmosphere has been lost. The H_2O -atmosphere stage (“ii”) is long because the H_2O atmosphere is buffered by the large dissolved-in-magma H_2O reservoir.

side of Figure 1), within our model H_2 is added to the model planet, and magma–atmosphere interaction occurs, forming H_2O . The initial H_2 mass is specified such that the model atmospheric pressure (following magma–atmosphere interaction) is 5 kbar. The resulting model sub-Neptune has $\mu_{\text{atm}} \approx 3$, $X_{\text{FeO}} = 6$ wt%, and a radius of roughly $\sim 1.9 R_{\oplus}$ (Lopez & Fortney 2014). $\sim 1.9 R_{\oplus}$ worlds are underabundant in the exoplanet census, and there is strong statistical evidence that this is due to atmospheric loss, forming $R < 1.7 R_{\oplus}$ planets (e.g., Rogers & Owen 2020).

Driven by atmospheric loss, the model atmosphere quickly thins from 5 kbar to 200 bar. At this point almost all of the H_2 has been removed and the atmosphere is H_2O -dominated ($\mu_{\text{atm}} > 10$; Figure 1). Thereafter, despite ongoing atmospheric loss, the rate of atmospheric pressure decline greatly decreases (inflection in Figure 1, top panel, note log scale). This is because H_2O outgasses from the magma. The atmosphere stays water-dominated and buffered (in this run) to 10–100 bar (comparable to an Earth ocean mass of H_2O) for a long time. The H_2O is not derived from solid volatiles (hydrated minerals or ice). Instead, it is produced on the planet—endogenous water. The total mass that must be removed to devolatilize the planet is $\sim 10\times$ the maximum mass of the atmosphere.

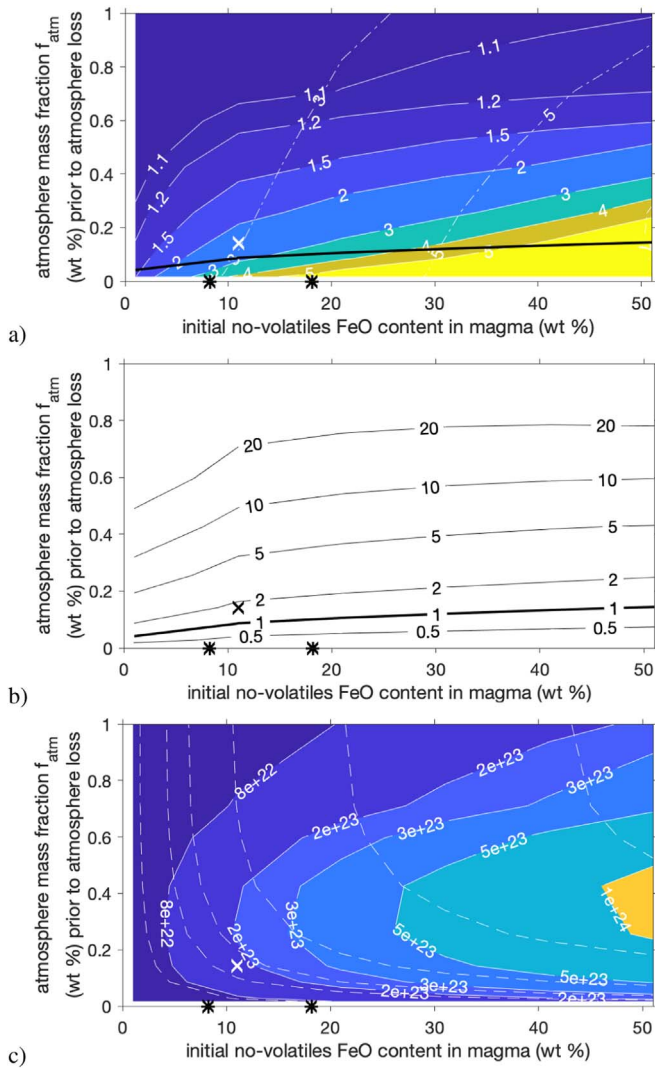


Figure 2. Results for $5 M_{\oplus}$ simulations. (a) Colors and solid contours correspond to the ratio, χ , of the mass removal (kg) necessary to dry out an endogenous waterworld (combined width of stages “i” and “ii” in Figure 1), to the mass removal needed to remove the H_2 envelope from the planet and raise μ_{atm} above 10 (width of stage “i” on Figure 1). Dashed contours correspond to μ_{atm} before any atmospheric loss has occurred. The cross corresponds to the Figure 1 simulation. The black line is the stoichiometric threshold below which enough FeO is available to destroy all initial H_2O . Asterisks on the x-axis correspond to Earth (left) and Mars (right). (b) Moles of initial H_2O on the planet, normalized to the stoichiometric maximum (ignoring thermodynamics) H_2O that can be destroyed by reaction with FeO (reaction (6)). (c) Mass (kg) of H_2O that must be removed to dry out a wet super-Earth (width of stage “ii” on Figure 1). Dashed contours correspond to the same contours, but for initial H_2O mass (i.e., H_2O mass at the leftmost edge of Figure 1). Overall, for a wide range of parameters, a large initial mass of H_2O ensures a relatively lengthy stage with a 10–2000 bar, H_2O -dominated atmosphere.

(Water-dominated atmospheres up to 2000 bar are possible by this mechanism; Figure 2(c).) Most of this mass is removed while the planet is a super-Earth-sized, but water-enveloped world.

For a given star, planets very close to the star will evolve all the way to the right on Figure 1. Planets at large distances from the star will remain as H_2 -shrouded worlds with large radii and low densities (Rogers 2015). Planets at intermediate distances from the star will be water-enveloped super-Earths.

A relatively lengthy stage with a 10–2000 bar, H_2O -dominated atmosphere occurs for a wide range of parameters (Figure 2(a)). Only for model runs with $f_{\text{atm}} \gtrsim 0.6$ wt% is the water-enveloped

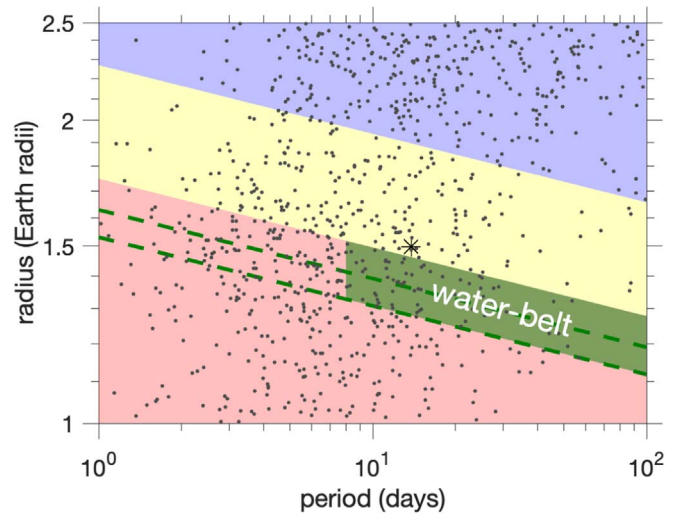


Figure 3. Predicted locations of endogenous waterworlds (green) in period-radius space. Planet data from Fulton & Petigura (2018) (the radius valley is in reality emptier than shown here, for <3 Gyr old stars). Black asterisk corresponds to Kepler-36b. Radius valley location (yellow) is from David et al. (2020). Red indicates super-Earth zone, and blue indicates sub-Neptune zone. Predicted endogenous waterworlds define a “water belt” lining the exoplanet radius valley. An initial f_{atm} of 0.43 wt% is assumed. The belt is wider for an initial no-volatiles FeO content in magma of 30 wt% (lower dashed line) than for 10 wt% (upper dashed line).

stage brief. According to models, $f_{\text{atm}} \gtrsim 0.6$ wt% worlds often stay as sub-Neptunes and do not become super-Earths (Rogers & Owen 2020). Earth-sized and larger planets should have an initial no-volatiles mantle FeO content of at least a few wt%. This is because Si from the mantle dissolves into the liquid-Fe core more readily than does mantle O, creating an excess of mantle O that pairs with Fe (Wordsworth et al. 2018). Indeed, Earth, Venus, and Mars have FeO mole fraction ~ 0.1 – 0.2 , and constraints on rocky extrasolar material from contaminated-white-dwarf data give an FeO mole fractions 0.1–0.5 (typically 0.15–0.35; Doyle et al. 2020). Mantle FeO contents of a few wt% or higher favor a water-enveloped stage in our model (Figure 2).

The typical atmospheric mass during the waterworld stage of a $5 M_{\oplus}$ simulation varies between simulations from $(1$ – $16) \times 10^{21}$ kg (corresponding to 100–2000 bar). The amount of H_2O that must be removed to desiccate the waterworld after reaching the high- μ_{atm} stage is much larger: 1–3 wt% of planet mass ($(2$ – $10) \times 10^{23}$ kg; Figure 2(c)). This is because H_2O is very soluble in magma.

4. Discussion

4.1. Which Hot Rocky Exoplanets Should Be Water-enveloped Today?

Endogenous-waterworld predictions can be made in planet radius–period space (Figure 3). In radius–period space, rocky exoplanets and sub-Neptunes are separated by a valley that is deficient in planets (Van Eylen et al. 2018; David et al. 2020; Petigura 2020). Atmospheric loss drives worlds vertically downward in Figure 3. Initially H_2 -shrouded worlds traverse the valley relatively rapidly as H_2 is lost (stage “i” in Figure 1). Worlds arrive at their near-final radii with 10–2000 bar H_2O -dominated atmospheres (stage “ii” in Figure 1). Whether or not the 10–2000 bar H_2O -dominated atmosphere is retained depends on the amount of irradiation and on M . A lower-mass core will lose more atmosphere for the same amount of

irradiation. This is because for less massive planets, the atmosphere is more weakly bound. Thus, for a given period (\approx irradiation), the radius valley corresponds to a threshold in planet mass (\approx planet core mass).

At orbital period $p = 32\text{--}64$ days, the paucity of super-Earths with radii $R = 1.3\text{--}1.6 R_{\oplus}$ ($\equiv 3\text{--}6 M_{\oplus}$) implies that $3\text{--}6 M_{\oplus}$ worlds are on average hydrogen-enveloped (and thus have radii $2\text{--}3 R_{\oplus}$; Rogers & Owen 2020).

In terms of our model, this implies that super-Earths in this period range that have radii just below the valley have received only a little bit more irradiation than is needed to remove all H_2 , and thus are in the endogenic-waterworld zone (stage “ii”). The same reasoning applies to $p = 8\text{--}32$ days if we assume that many cores have mass $>6 M_{\oplus}$ ($\equiv 1.6 R_{\oplus}$). At all periods, sufficiently low-mass worlds will be denuded of nebular-derived H (both as H_2 and as H_2O). If those low-mass worlds nevertheless have steam atmospheres, then the H_2O must be exogenic. In summary, if magma–atmosphere interaction is efficient, then endogenic waterworlds should line the exoplanet radius valley as it evolves over time (David et al. 2020).

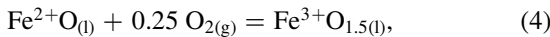
To make Figure 3, we make the additional, auxiliary assumption that the atmosphere loss process is energy-limited XUV-powered escape (e.g., Rogers & Owen 2020). Specifically,

$$\text{mass removed} = \int \frac{\eta L}{4a^2 G} \left(\frac{R^3}{M} \right) dt \propto R^{-0.7}, \quad (3)$$

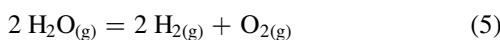
where η is efficiency, L is star XUV luminosity, a is semimajor axis, and G is the gravitational constant. To get the exponent $R^{-0.7}$, we approximate the atmosphere as thin, planet mass as constant, and $R \propto M^{0.27}$. If the atmosphere mass fraction at the sub-Neptune stage (prior to atmosphere loss) is a constant, then the amount of mass that must be removed scales as $R^{(1/0.27)}$. Then for a given a , the fractional extent to which volatile mass is removed scales as $R^{-(1/0.27)} R^{-0.7} = R^{-4.4}$. Then the lower edge of the water belt (radius of complete dessication, R_d) is approximated by $(R_v/R_d) = \chi^{1/4.4}$, where R_v is the radius of the lower edge of the valley, and χ is the waterworld multiplier factor from the $5 M_{\oplus}$ calculations (the quantity corresponding to the solid contours in Figure 2(a)). This is a simplification: χ varies with M , the atmosphere is not always thin, the location of the radius valley may vary with time (David et al. 2020), and other loss processes may be important. Nevertheless, this calculation shows that the number of planets that are predicted to be endogenous waterworlds can be large (Figure 3). Moreover, the predicted water belt includes super-Earths that (because of their large radius) are among the best targets for observations.

4.2. The Role of Selective Escape and Fe^{3+}

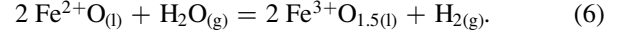
Loss of H_2 from the planet oxidizes the magma-plus-atmosphere system. Oxidation of Fe^{2+} to Fe^{3+} ,



combined with the (thermodynamically disfavored) water-breakdown reaction



yields the water-destroying reaction



Reaction (6) can be important for secondary atmospheres (Schaefer et al. 2016; Wordsworth et al. 2018). However, two effects limit its importance for sub-Neptune-to-super-Earth conversion. First, worlds with initial (postreaction, preloss) atmosphere mass fractions $f_{\text{atm}} > 0.1$ wt% do not have enough moles of FeO to convert most of the H_2O back to H_2 (Figure 2). Moreover, 0.1 wt% is close to the minimum f_{atm} for a super-Earth that is imbedded in the nebula (Ginzburg et al. 2016). Therefore it is possible that for real planets FeO oxidation is not enough to destroy much H_2O . Second, the ratio of products to reactants for reaction (6) is given by the equilibrium constant K_3 :

$$K_3 = \frac{a\text{FeO}_{1.5}^2 f_{\text{H}_2}}{a\text{FeO}^2 f_{\text{H}_2\text{O}}}, \quad (7)$$

where a denotes chemical activity (effective concentration) and f denotes fugacity (bar). For $1500 \text{ K} < T < 4000 \text{ K}$, using standard thermodynamics data supplemented by data from Lange & Carmichael (1987) and Zhang et al. (2017), we obtain $K_3 \sim 10^{-3}$. Thus, if the atmospheric $\text{H}_2/\text{H}_2\text{O}$ ratio rises above 10^{-3} , then Equation (7) implies that the mantle Fe must be mostly FeO (and not $\text{FeO}_{1.5}$). Thus, reaction (6) self-limits.

Water destruction by reaction (6) is most effective if the atmospheric $\text{H}_2/\text{H}_2\text{O}$ ratio is driven below 10^{-3} by selective H escape. Selective H escape at the diffusion limit (assuming a homopause composition of 2/3 H and 1/3 O) allows water destruction at a rate of $\sim 3 \times 10^{22} \text{ kg Gyr}^{-1}$ (Wordsworth et al. 2018). This limit permits enough H escape to overcome the Fe^{2+} sink for many worlds below the thick black line in Figure 2(b). Whether or not this upper limit is approached over the lifetime of the planet will depend on the XUV flux, among other factors (Wordsworth et al. 2018). If all H_2O is destroyed, the end state is a solid surface rich in the Fe^{3+} minerals, such as magnetite and hematite.

Worlds above the thick black line in Figure 2 do not have enough FeO to reduce all the water. For these worlds, if Fe^{2+} is completely oxidized to Fe^{3+} , then further selective H escape leaves behind an atmosphere enriched in O_2 (e.g., Wordsworth et al. 2018).

4.3. Uncertainties and Limitations

Some magma–atmosphere interaction is unavoidable. The magma is almost inviscid and as the magma–atmosphere interface is depressurized and cooled, bubbles and cold boundary layers form, and these stir up deeper magma. However, we do not know if the magma ocean is well-stirred enough that each magma parcel equilibrates with the atmosphere at the maximum atmospheric pressure. (A sensitivity test reducing the volume of magma that interacts with the atmosphere three-fold causes a roughly two-fold reduction in the relative length of the water-dominated stage.) An alternative endmember hypothesis is that sub-Neptunes’ cores are stratified (Ormel et al. 2021).

An intermediate possibility is that magma–atmosphere interaction occurs gigayears after planet formation. Magma–atmosphere interaction can cause factor-of-several changes in f_{atm} even without atmospheric loss (Kite et al. 2020). Perhaps this contributes to the formation and evolution of the radius

valley. Delaying magma–atmosphere interaction until most of the atmosphere has already been lost drives planets down on the plots in Figure 2, making magnetite/hematite surfaces more likely. These possibilities motivate more research on mixing within magma oceans on sub-Neptunes.

As the atmosphere shifts from H_2 -dominated to H_2O -dominated, the efficiency with which loss drivers are converted into mass loss might decrease (Johnstone et al. 2018; Johnstone 2020). This does not affect our conclusions.

We approximate magma–atmosphere interface temperature and within-envelope gravitational acceleration as constant during atmosphere loss (2500 K and 1.2^{-2} of the interface value, respectively). We neglect changes in the fugacity coefficient during atmosphere loss (Kite et al. 2019). For this study, these effects are small relative to that of H_2O 's greater solubility.

We ignore magma–ocean solidification, which pushes volatiles into the atmosphere as the magma surface cools (Turbet et al. 2020).

The starting point for our calculations is the results of Kite et al. (2020). The most important limitation of that study is that material property data (e.g., solubilities) are based on a relatively small number of laboratory and/or numerical experiments.

Recent work indicates magma Fe^{2+} disproportionates at high pressure (Armstrong et al. 2019). This process leads to a more-oxidized magma and more-oxidized atmosphere, supporting our conclusion (Armstrong et al. 2019).

We ignore gases other than H_2 and H_2O . This is justified because C species are sparingly soluble in magma (Keppler & Golabek 2019), so they are not protected by dissolution in the magma. Instead they are lost with the H_2 .

4.4. Tests and Implications

We describe three possible tests of our model's predictions (Figure 3).

(1) Whereas hot rocky exoplanets with solid-derived volatiles should have volatile $\text{C}/\text{O} \sim 1$ (Bitsch et al. 2019), endogenous waterworlds should have lower volatile C/O ratio, with atmospheres that are $>50\%$ H_2O by number. This hypothesis can be tested using spectroscopic observations (e.g., Benneke et al. 2019).

(2) The 10–2000 bar atmospheres predicted by our model are 150–500 km thick (according to Turbet et al. 2020), enough to make a $1.5 R_{\oplus}$ planet less dense relative to an Earth-like composition by up to 17%. A statistical test of this prediction is imminently possible. Already, radial-velocity data for transiting super-Earths (Sinukoff 2018; Otegi et al. 2020) show a clump with densities too low for Earth-like composition. These densities imply an atmosphere, because although they are consistent with spheres of pure MgSiO_3 , cosmochemically plausible bare-rock planets contain Fe and so are denser. Whether this clump in the data is real or not awaits a detailed analysis correcting for detection biases. Our model predicts that more massive rocky planets will show this density anomaly more frequently.

(3) Tests for predicted atmospheres can be done using phase curves or measurements of secondary-eclipse depth (e.g., Koll et al. 2019; Kreidberg et al. 2019; Mansfield et al. 2019). These methods do not require detection of atmospheric molecules. A survey of ~ 10 rocky exoplanets within the water belt in

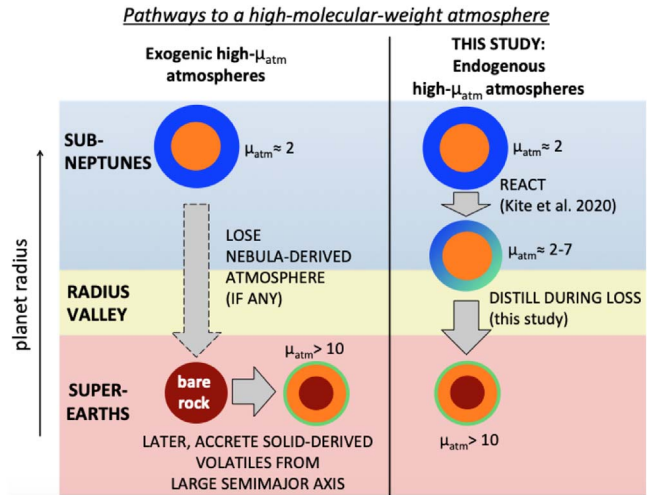


Figure 4. Graphical abstract of this Letter. Blue and green shading corresponds to low-molecular-weight species and high-molecular-weight species, respectively. Our proposed scenario provides an alternative route to producing high-mean-molecular-weight atmospheres on hot rocky exoplanets. The hot super-Earth population could contain both types of atmospheres.

Figure 3 would be sufficient to test the prediction that most have atmospheres.

If endogenous high- μ_{atm} worlds are common, then implications include the following. (1) Water envelopes can be made in situ, so water is not a proxy for migration of solid-derived volatiles across the snowline. (2) Many bare-rock worlds will have surfaces rich in the Fe^{3+} -bearing, spectroscopically distinctive minerals magnetite and hematite (Mansfield et al. 2019). (3) Since endogenous waterworlds imply magma–atmosphere interaction, the magma–atmosphere interaction explanation for the sharp drop-off in exoplanet abundance above $3 R_{\oplus}$ (Kite et al. 2019) would be favored. (4) Endogenous water formation should work as well or better in the habitable zone. Therefore, habitable-zone worlds that have H_2O with nebula-sourced H with nebula-sourced H will be common (Ikoma & Genda 2006).

5. Summary and Conclusion

In our model, adding and then removing a H_2 atmosphere draws out a H_2O atmosphere (Figure 4). This outcome can be understood as follows: (1) Early magma–atmosphere reaction transfers electrons from H_2 to Fe^{2+} , forming dense Fe^0 metal that sinks to the liquid-iron core. This oxidation of the magma–atmosphere system is irreversible because (by assumption) chemical re-equilibration between the liquid-iron core and the magma is forbidden. (2) The H_2O atmosphere is buffered by dissolved H_2O . The dissolved reservoir is massive because H_2O is soluble in magma and because the $\text{FeO}-\text{H}_2$ reaction volatilizes the oxygen from the magma, which increases the mass of volatiles. Our result is different from that of Kite & Barnett (2020), which traced the fate of a hypothetical 10^{21} kg dose of solid-derived volatiles, simply because the mass of H_2O is so much larger.

In conclusion, if magma–atmosphere interaction is efficient early in a sub-Neptune's history, then during sub-Neptune-to-super-Earth conversion $>80\%$ of the reduction in atmospheric volume occurs while most of the volatile mass remains. Thus, location below the radius valley does not imply bare-rock status. Instead, super-Earths can maintain 150–500 km thick

(10–2000 bar) H₂O atmospheres, buffered by a large reservoir of dissolved-in-magma H₂O. The H₂O is assembled from nebula-derived H and magma-sourced O. The main weakness of the idea is that we do not know if magma–atmosphere interaction is efficient on small sub-Neptunes. The main strength of the endogenous-waterworld hypothesis is that it is imminently testable.

We thank B. Fegley and E. Ford. We thank the anonymous reviewer for comments that substantially improved the presentation of the results. Grant: NASA (NNX16AB44G).

Code availability. All code can be obtained for unrestricted further use by emailing E.S.K.

ORCID iDs

Edwin S. Kite  <https://orcid.org/0000-0002-1426-1186>

Laura Schaefer  <https://orcid.org/0000-0003-2915-5025>

References

- Armstrong, K., Frost, D. J., McCammon, C. A., et al. 2019, *Sci*, **365**, 903
- Bean, J. L., Raymond, S. N., & Owen, J. E. 2020, *JGRE*, **126**, e2020JE006639
- Benneke, B., Knutson, H. A., Lothringer, J., et al. 2019, *NatAs*, **3**, 813
- Bitsch, B., Raymond, S. N., & Izidoro, A. 2019, *A&A*, **624**, A109
- Dai, F., Masuda, K., Winn, J. N., et al. 2019, *ApJ*, **883**, 79
- David, T. J., Contardo, G., Sandoval, A., et al. 2020, arXiv:2011.09894
- Doyle, A. E., Klein, B., Schlichting, H. E., et al. 2020, *ApJ*, **901**, 10
- Elkins-Tanton, L. T., & Seager, S. 2008b, *ApJ*, **688**, 628
- Fulton, B. J., & Petigura, E. A. 2018, *AJ*, **156**, 264
- Ginzburg, S., Schlichting, H. E., & Sari, R. 2016, *ApJ*, **825**, 29
- Hirschmann, M. M., Withers, A. C., Ardia, P., et al. 2012, *E&PSL*, **345**, 38
- Hsu, D. C., Ford, E. B., Ragozzine, D., et al. 2019, *AJ*, **158**, 109
- Hu, R., Seager, S., & Yung, Y. L. 2015, *ApJ*, **807**, 8
- Ikoma, M., & Genda, H. 2006, *ApJ*, **648**, 696
- Johnstone, C. P. 2020, *ApJ*, **890**, 79
- Johnstone, C. P., Güdel, M., Lammer, H., et al. 2018, *A&A*, **617**, A107
- Keppler, H., & Golabek, G. 2019, *Geochemical Perspectives Letters*, **11**, 12
- Kite, E. S., & Barnett, M. 2020, *PNAS*, **117**, 18264
- Kite, E. S., Fegley, B., Schaefer, L., et al. 2019, *ApJL*, **887**, L33
- Kite, E. S., Fegley, B., Schaefer, L., et al. 2020, *ApJ*, **891**, 111
- Koll, D., Malik, M., Mansfield, M., et al. 2019, *ApJ*, **886**, 140
- Kreidberg, L., Koll, D., Morley, C., et al. 2019, *Natur*, **573**, 87
- Lange, R. A., & Carmichael, I. S. E. 1987, *GeCoA*, **51**, 2931
- Lopez, E. D., & Fortney, J. J. 2014, *ApJ*, **792**, 1
- Mansfield, M., Kite, E. S., Hu, R., et al. 2019, *ApJ*, **886**, 141
- Ormel, C., Vazan, A., & Brouwers, M. 2021, *A&A*, in press
- Otegi, J. F., Bouchy, F., & Helled, R. 2020, *A&A*, **634**, A43
- Papale, P. 1997, *CoMP*, **126**, 237
- Petigura, E. A. 2020, *AJ*, **160**, 89
- Rogers, J. G., & Owen, J. E. 2020, arXiv:2007.11006
- Rogers, L. A. 2015, *ApJ*, **801**, 41
- Sasaki, S. 1990, in *Origin of the Earth*, ed. H. Newsom & J. H. Jones (Oxford: Oxford Univ. Press), 195
- Schaefer, L., Wordsworth, R. D., Berta-Thompson, Z., et al. 2016, *ApJ*, **829**, 63
- Sinukoff, E. 2018, PhD thesis, U. Hawaii
- Turbet, M., Bolmont, E., Ehrenreich, D., et al. 2020, *A&A*, **638**, A41
- Van Eylen, V., Agentoft, C., Lundkvist, M. S., et al. 2018, *MNRAS*, **479**, 4786
- Wordsworth, R. D., Schaefer, L. K., & Fischer, R. A. 2018, *AJ*, **155**, 195
- Zhang, H. L., Hirschmann, M. M., Cottrell, E., et al. 2017, *GeCoA*, **204**, 83